2021 American Control Conference (ACC)
New Orleans, USA, May 25-28, 2021

Retrospective Cost Adaptive Harmonic Disturbance Rejection Using Dereverberated Target Models

Nima Mohseni[1] and Dennis S. Bernstein[1]

Abstract— **The present paper focuses on adaptive feedback disturbance rejection for high-order, lightly damped systems using retrospective cost adaptive control (RCAC). RCAC requires a closed-loop target model, which captures key features of the plant dynamics. In the SISO case, this information includes knowledge of the sign of the leading numerator coefficient, relative degree, and non-minimum phase zeros. The present paper investigates the feasibility of using a deverberated transfer function (DTF) as the closed-loop target model. A dereverberated model of a lightly damped plant captures the magnitude and phase trend but ignores resonances and anti-resonances, thus providing a simplified, low-order model of a lightly damped system. The present paper investigates the performance and robustness of RCAC using a dereverberated target model based on the nominal plant model.**

I. Introduction

Disturbance rejection for high-order, lightly damped structures and acoustic spaces is a longstanding challenge in control theory and technology [1], [2], [3]. Applications of this technology range from space apertures (optical and RF) to positioning mechanisms in hard drives [4], [5]. The difficulty of the problem stems from the high dimensionality—theoretically infinite—of the plant dynamics, the proximity of the poles to the imaginary axis, the presence of non-minimum phase zeros, and model uncertainty due to limitations in analytical and empirical modeling. Additional challenges arise from loop coupling in MIMO applications, time delays in wave propagation, limitations in sensors, actuators, and computation, and spectral and spatial spillover.

Although feedback control can modify the dynamics of a structure, for example, by adding damping or altering mode shapes, this approach has inherent limitations [6] and can destabilize the system. In view of these challenges, an alternative approach is to use adaptive feedforward disturbance rejection, which uses a measurement of the disturbance or a closely related sensor signal, such as an engine tachometer. One of the most popular feedforward control algorithms for adaptive disturbance rejection is filtered-x least-mean-square (FxLMS) [3], [7], [8], which uses knowledge of the secondary-path (control-to-error-signal) dynamics to update the coefficients of a finite-impulse response (FIR) controller.

In situations where feedforward disturbance rejection is not applicable, feedback control is of interest. Fixed-gain, feedback control methods, including optimal and robust techniques, have been widely studied [9]. Uncertainty in the high-order, lightly damped dynamics, however, motivates the need for developing adaptive feedback control techniques.

The present paper focuses on adaptive feedback disturbance rejection for high-order, lightly damped systems using retrospective cost adaptive control (RCAC). RCAC is a direct, digital adaptive control technique for disturbance rejection for plants with uncertain dynamics and disturbance spectrum [10]. As shown in [10], RCAC requires a *closed-loop target model*, which captures key features of the plant dynamics. In the SISO case, this information includes knowledge of the sign of the leading numerator coefficient, relative degree, and non-minimum phase zeros. In the MIMO case, the required information is obtained through a collection of impulse-response matrices [11].

The goal of the present paper is to determine the feasibility of using a *deverberated transfer function (DTF)* as the closed-loop target model. Roughly speaking, a dereverberated model of a lightly damped plant captures the magnitude and phase trend but ignores resonances and anti-resonances [12], [13], [14]. Consequently, a DTF provides a simplified, low-order model of a lightly damped system. The present paper investigates the performance and robustness of RCAC using a dereverberated target model based on the nominal plant model.

Various techniques have been developed to generate a DTF from an analytical or empirical plant model [15], [16], [17], [18]. All these techniques capture some aspect of the mean of the frequency response, for example, by optimizing the logarithmic-average of the magnitude of the frequency response.

The paper is structured as follows. Section II explains the disturbance rejection problem investigated in this paper, and the RCAC algorithm. Section III covers construction of the closed-loop target model used in RCAC and the modifications that are needed to be able to use a dereverberated target model. We then present a method for generating a DTF in Section IV. Section V investigates harmonic disturbance rejection using RCAC for a numerical example. Finally, adaptive control of a MISO acoustic experiment using a MISO dereverberated target model is described in Section VI.

II. Retrospective Cost Adaptive Control

A. Sampled-Data Disturbance-Rejection Problem

The disturbance rejection problem involves four signals, namely, the performance z, the disturbance w, the output y, and the control u. These signals are related by the transfer functions G_{zu}, G_{zw}, G_{yu}, and G_{yw}, which define the continuous-time, input-output model

$$z(t) = G_{zw}(\mathbf{p})w(t) + G_{zu}(\mathbf{p})u(t), \tag{1}$$

$$y(t) = G_{yw}(\mathbf{p})w(t) + G_{yu}(\mathbf{p})u(t), \tag{2}$$

where $\mathbf{p}$ is the differentiation operator $\mathrm{d}/\mathrm{d}t$. The signals $y(t)$ and $z(t)$ are sampled instantaneously to obtain $y_k \triangleq y(kT_\mathrm{s}) \in \mathbb{R}^{l_y}$ and $z_k \triangleq z(kT_\mathrm{s}) \in \mathbb{R}^{l_z}$, and the control $u(t) \equiv u_k \in \mathbb{R}^{l_u}$ for all $t \in [kT_\mathrm{s}, (k+1)T_\mathrm{s})$ is reconstructed from u_k using a zero-order hold (ZOH). The feedback controller $G_\mathrm{c}(\mathbf{q}, \hat{\theta})$, where $\mathbf{q}$ is the forward-shift operator and $\hat{\theta}$ is a vector of controller coefficients that is updated at each step,

[1]Department of Aerospace Engineering, The University of Michigan, Ann Arbor, MI 48109, USA

uses y_k to determine u_k, as shown in Figure 1. In order to suppress the effect of the disturbance $w(t)$ on z_k, the adaptive controller uses measurements of z_k to update $G_{\rm c}(\mathbf{q},\hat{\theta})$. The controller update is indicated by the diagonal line in Figure 1,

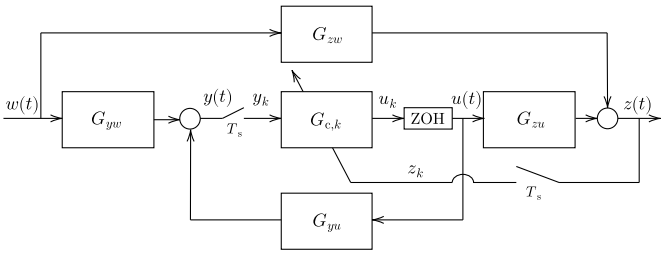

Fig. 1: Block diagram of the sampled-data adaptive disturbance rejection architecture. The controller $G_{{\rm c},k}$ is updated at each time step k.

It follows from (1) and (2) that z_k and y_k are given by

$$z_k = z_{w,k} + G_{zu,{\rm d}}(\mathbf{q})u_k, \tag{3}$$

$$y_k = y_{w,k} + G_{yu,{\rm d}}(\mathbf{q})u_k, \tag{4}$$

where

$$z_{w,k} \triangleq C_{zw}\int_{(k-1)T_{\rm s}}^{kT_{\rm s}} e^{A_{zw}(kT_{\rm s}-t)}B_{zw}w(t)\,{\rm d}t + D_{zw}\int_{(k-1)T_{\rm s}}^{kT_{\rm s}} w(t)\,{\rm d}t, \tag{5}$$

$$y_{w,k} \triangleq C_{yw}\int_{(k-1)T_{\rm s}}^{kT_{\rm s}} e^{A_{yw}(kT_{\rm s}-t)}B_{yw}w(t)\,{\rm d}t + D_{yw}\int_{(k-1)T_{\rm s}}^{kT_{\rm s}} w(t)\,{\rm d}t, \tag{6}$$

where $(A_{zw},B_{zw},C_{zw},D_{zw})$ and $(A_{yw},B_{yw},C_{yw},D_{yw})$ are realizations of $G_{zu}(\mathbf{p})$ and $G_{yu}(\mathbf{p})$, respectively, and $G_{zu,{\rm d}}(\mathbf{q})$ and $G_{yu,{\rm d}}(\mathbf{q})$ are the zero-order-hold discretizations of $G_{zu}(\mathbf{p})$ and $G_{yu}(\mathbf{p})$, respectively. A block diagram of the discrete-time disturbance-rejection problem is shown in Figure 2.

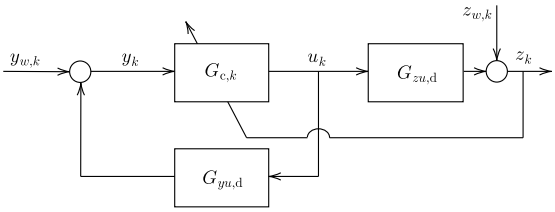

Fig. 2: Block diagram of the sampled-data adaptive disturbance rejection architecture in discrete time.

B. RCAC Algorithm

For the current vector θ_k of controller coefficients, $G_{\rm c}(\mathbf{q},\theta_k)$ is realized by the linear, time-varying, input-output model

$$u_k = \sum_{i=1}^{n_{\rm c}} P_{i,k}u_{k-i} + \sum_{i=1}^{n_{\rm c}} Q_{i,k}y_{k-i} \tag{7}$$

where $P_{i,k}\in\mathbb{R}^{l_u\times l_u}$, $Q_{i,k}\in\mathbb{R}^{l_u\times l_y}$, and $n_{\rm c}$ is the controller order. The startup protocol for (7) is given by

$$u_k = \begin{cases} 0, & k < k_{\rm w}, \\ \Phi_k\theta_k, & k \geq k_{\rm w} \end{cases} \tag{8}$$

where the regressor matrix Φ_k is defined as

$$\Phi_k \triangleq \begin{bmatrix} u_{k-1} \\ \vdots \\ u_{k-n_{\rm c}} \\ y_{k-1} \\ \vdots \\ y_{k-n_{\rm c}} \end{bmatrix}^{\rm T} \otimes I_{l_u} \in \mathbb{R}^{l_u\times l_\theta}, \tag{9}$$

$k_w \geq n_{\rm c}$ is the number of steps to wait while Φ_k is being populated with data, θ_k is the controller coefficient vector defined as

$$\theta_k \triangleq \mathrm{vec}\,[P_{1,k}\ \cdots\ P_{n_{\rm c},k}\ Q_{1,k}\ \cdots\ Q_{n_{\rm c},k}]^{\rm T} \in \mathbb{R}^{l_\theta}, \tag{10}$$

and $l_\theta \triangleq n_{\rm c}l_u(l_u+l_y)$.

The retrospective performance variable is defined by

$$\hat{z}_k(\hat{\theta}) \triangleq z_k - G_{\rm f}(\mathbf{q})(u_k - \Phi_k\hat{\theta}), \tag{11}$$

where $\hat{\theta}$ is the controller coefficient vector to be optimized, and $G_{\rm f}(\mathbf{q})\in\mathbb{R}^{l_z\times l_u}$ is a filter. As discussed in Subsection II-D, $G_{\rm f}$ plays the role of the target model for a closed-loop transfer function. Defining the filtered quantities $u_{{\rm f},k} \triangleq G_{\rm f}(\mathbf{q})u_k$ and $\Phi_{{\rm f},k} \triangleq G_{\rm f}(\mathbf{q})\Phi_k$, (11) can be written as

$$\hat{z}_k(\hat{\theta}) = z_k - (u_{{\rm f},k} - \Phi_{{\rm f},k}\hat{\theta}). \tag{12}$$

The controller coefficient vector θ_k is updated by minimizing the cost function

$$J_k(\hat{\theta}) \triangleq \frac{1}{2}(\hat{z}_k(\hat{\theta})^{\rm T}\hat{z}_k(\hat{\theta}) + \hat{\theta}^{\rm T}R\hat{\theta}), \tag{13}$$

where the positive-definite matrix $R\in\mathbb{R}^{l_\theta\times l_\theta}$ is a regularization term. Using gradient descent, the update law for the controller coefficient vector is given by

$$\theta_{k+1} = \theta_k - \mu_k(\Phi_{{\rm f},k}^{\rm T}\hat{z}_k(\theta_k) + R\theta_k) \tag{14}$$

where μ_k is the adaptive step size. For computational convenience, the step size is chosen to be

$$\mu_k = \frac{\alpha}{\|\Phi_{{\rm f},k}\|_{\rm F}^2 + \epsilon}, \tag{15}$$

where $\|\cdot\|_{\rm F}$ is the Frobenius norm, ϵ is a small positive nonzero term, and $\alpha > 0$ is chosen to adjust the speed of the adaptation.

C. Analysis of the Closed-Loop System

Defining

$$\overline{u}_k(\hat{\theta}) \triangleq \Phi_k\hat{\theta}, \tag{16}$$

$$\tilde{u}_k(\hat{\theta}) \triangleq u_k - \overline{u}_k(\hat{\theta}) = u_k - \Phi_k\hat{\theta}, \tag{17}$$

(11) can be written as

$$\hat{z}_k(\hat{\theta}) = z_k - G_{\rm f}(\mathbf{q})\tilde{u}_k(\hat{\theta}). \tag{18}$$

Next, using (7) and (17), the controller $G_{\rm c}(\mathbf{q},\hat{\theta})$ corresponding to $\hat{\theta}$ is realized as

$$\overline{u}_k(\hat{\theta}) = \sum_{i=1}^{n_{\rm c}} \hat{P}_i \overline{u}_{k-i}(\hat{\theta}) + \sum_{i=1}^{n_{\rm c}} \hat{P}_i \tilde{u}_{k-i}(\hat{\theta}) + \sum_{i=1}^{n_{\rm c}} \hat{Q}_i y_{k-i}, \tag{19}$$

which implies that

$$\overline{u}_k(\hat{\theta}) = D_{\rm c}^{-1}(\mathbf{q},\hat{\theta})[(\mathbf{q}^{n_{\rm c}} I_{l_u} - D_{\rm c}(\mathbf{q},\hat{\theta}))\tilde{u}_k(\hat{\theta}) + N_{\rm c}(\mathbf{q},\hat{\theta}) y_k], \tag{20}$$

where

$$N_{\rm c}(\mathbf{q},\hat{\theta}) \triangleq \mathbf{q}^{n_{\rm c}-1}\hat{Q}_1 + \cdots + \hat{Q}_{n_{\rm c}}, \tag{21}$$

$$D_{\rm c}(\mathbf{q},\hat{\theta}) \triangleq \mathbf{q}^{n_{\rm c}} I_{l_u} - \mathbf{q}^{n_{\rm c}-1}\hat{P}_1 - \cdots - \hat{P}_{n_{\rm c}}. \tag{22}$$

Next, defining

$$G_{\rm c}(\mathbf{q},\hat{\theta}) \triangleq D_{\rm c}^{-1}(\mathbf{q},\hat{\theta}) N_{\rm c}(\mathbf{q},\hat{\theta}) \tag{23}$$

and substituting (17) and (20) into (3) and (4) and solving for the closed-loop response of z_k yields

$$z_k = \xi_k(\hat{\theta}) + \tilde{G}_{z\tilde{u}}(\mathbf{q},\hat{\theta})\tilde{u}_k(\hat{\theta}), \tag{24}$$

where

$$\xi_k(\hat{\theta}) \triangleq z_{w,k} + G_{zu,{\rm d}}(\mathbf{q}) G_{\rm c}(\mathbf{q},\hat{\theta})(I_{l_y} - G_{yu,{\rm d}}(\mathbf{q}) G_{\rm c}(\mathbf{q},\hat{\theta}))^{-1} y_{w,k}, \tag{25}$$

$$\tilde{G}_{z\tilde{u}}(\mathbf{q},\hat{\theta}) \triangleq \mathbf{q}^{n_{\rm c}} G_{zu,{\rm d}}(\mathbf{q}) \big(D_{\rm c}^{-1}(\mathbf{q},\hat{\theta}) + G_{\rm c}(\mathbf{q},\hat{\theta})[I_{l_y} - G_{yu,{\rm d}}(\mathbf{q}) G_{\rm c}(\mathbf{q},\hat{\theta})]^{-1} G_{yu,{\rm d}}(\mathbf{q}) D_{\rm c}^{-1}(\mathbf{q},\hat{\theta}) \big). \tag{26}$$

Note that $\xi_k(\hat{\theta})$ is the portion of the measurement z_k due to $w(t)$ when using the controller $G_{\rm c}(\mathbf{q},\hat{\theta})$. Finally, note that (16)–(26) are valid for all $\hat{\theta} \in \mathbb{R}^{l_\theta}$.

D. Optimal Controller and the Closed-Loop Target Model

From [10], assuming that for all $k \geq 0$, there exists a θ^* where $\xi_k(\theta^*) \approx 0$, and sufficient persistence of excitation such that (14) converges to θ^*, it can be shown that minimizing (13) is equivalent to fitting $\tilde{G}_{z\tilde{u}}(\mathbf{q},\theta_{k+1})$ to $G_{\rm f}(\mathbf{q})$. Consequently, $G_{\rm f}(\mathbf{q})$ serves as a closed-loop target model for $\tilde{G}_{z\tilde{u}}(\mathbf{q},\theta^*)$.

In the case where y_k, z_k, and u_k are scalar, $\tilde{G}_{z\tilde{u}}(\mathbf{q},\theta_{k+1})$ can be written as

$$\tilde{G}_{z\tilde{u}}(\mathbf{q},\theta_{k+1}) = \frac{\mathbf{q}^{n_c} N_{zu,{\rm d}}(\mathbf{q})}{D(\mathbf{q}) D_{\rm c}(\mathbf{q},\theta_{k+1}) - N_{yu,{\rm d}}(\mathbf{q}) N_{\rm c}(\mathbf{q},\theta_{k+1})}, \tag{27}$$

where $G_{zu,{\rm d}}(\mathbf{q}) = N_{zu,{\rm d}}(\mathbf{q})/D(\mathbf{q})$ and $G_{yu,{\rm d}}(\mathbf{q}) = N_{yu,{\rm d}}(\mathbf{q})/D(\mathbf{q})$. Note that the zeros of $\tilde{G}_{z\tilde{u}}(\mathbf{q},\theta_{k+1})$ include the zeros of $G_{zu,{\rm d}}(\mathbf{q})$. Although these zeros do not depend on $G_{\rm c}(\mathbf{q},\theta_{k+1})$, they can be canceled by roots of the denominator of $\tilde{G}_{z\tilde{u}}(\mathbf{q},\theta_{k+1})$. In the case of NMP zeros, this cancellation represents a hidden instability due to the cascade interconnection between the plant and $G_{\rm c}(\mathbf{q},\theta_{k+1})$ [19]. As shown in [10], this cancellation can be prevented by ensuring that all the NMP zeros of $G_{zu}(\mathbf{q})$ are also zeros of $G_{\rm f}(\mathbf{q})$. Unfortunately, this requires knowledge of all the NMP zeros of $G_{zu}(\mathbf{q})$. Section III-B considers a derverberated approximation of $G_{zu}(\mathbf{q})$ that alleviates this requirement.

III. Construction of the Closed-Loop Target Model

A. Standard Construction of the Closed-Loop Target Model

In the SISO case, note that the relative degree of $\tilde{G}_{z\tilde{u}}(\mathbf{q},\theta_{k+1})$ is equal to the relative degree of $G_{zu,{\rm d}}(\mathbf{q})$. Therefore, in order to facilitate model matching between $\tilde{G}_{z\tilde{u}}(\mathbf{q},\theta_{k+1})$ and $G_{\rm f}(\mathbf{q})$, we choose the relative degree of $G_{\rm f}(\mathbf{q})$ to be equal to the relative degree of $G_{zu,{\rm d}}(\mathbf{q})$. For the same reason, we also construct $G_{\rm f}(\mathbf{q})$ to have the same leading numerator coefficient as $G_{zu,{\rm d}}(\mathbf{q})$.

Furthermore, it can be seen that the numerator of $\tilde{G}_{z\tilde{u}}(\mathbf{q},\theta_{k+1})$ contains all the zeros present in $G_{zu,{\rm d}}(\mathbf{q})$. Therefore, as the target-model matching performance is minimized, any NMP zeros that are present in $G_{zu,{\rm d}}(\mathbf{q})$, but not in $G_{\rm f}(\mathbf{q})$ can lead to unstable pole-zero cancellation. Therefore, $G_{\rm f}(\mathbf{q})$ must be constructed such that all the NMP zeros of $G_{zu,{\rm d}}(\mathbf{q})$ are present in $G_{\rm f}(\mathbf{q})$.

A straightforward technique for constructing $G_{\rm f}(\mathbf{q})$ that satisfies these requirements in the SISO case is given by

$$G_{\rm f}(\mathbf{q}) = \sum_{i=0}^{n_{\rm f}} \frac{H_i}{\mathbf{q}^i}, \tag{28}$$

where H_i is the ith the Markov parameter of $G_{zu,{\rm d}}(\mathbf{q})$ and $n_{\rm f}$ is the order of $G_{\rm f}(\mathbf{q})$.

Note that the FIR transfer function (28) is a truncated Laurent expansion of $G_{zu,{\rm d}}(\mathbf{q})$ [11]. Therefore, by choosing a sufficiently large value of $n_{\rm f}$, $G_{zu,{\rm d}}(\mathbf{q})$ provides an approximation of $G_{zu,{\rm d}}(\mathbf{q})$ that is useful in the MIMO case. In the case where the plant is minimum phase and asymptotically stable, only the first nonzero Markov parameter is used in the summation. Unfortunately, for lightly damped systems, several hundred Markov parameters may be needed to approximate the NMP zeros; this number is prohibitively large in applications. To overcome this difficulty, we use a dereverberated transfer function as the closed-loop target model.

B. Construction of the Dereverberated Target Model

Section IV describes a method for constructing a dereverberated transfer function (DTF). Using a DTF as described in Section IV for the closed-loop target model leads to poor disturbance rejection performance. However, only a simple adjustment to the DTF is needed to alleviate the poor performance. The adjusted DTF that is used as the target model $G_{\rm f}$ is termed the dereverberated target model (DTM). In particular, we set

$$G_{\rm f}(z) = \beta \widehat{G}_{\rm d}(z), \tag{29}$$

where $\beta \in (0,1]$.

IV. Identification of a Dereverberated Transfer Function

A. Complex Windowed Averaging

The dereverberated transfer function can be constructed by smoothing the frequency response of $G_{\rm d}(z)$ with a windowed average and using the resulting smoothed frequency response to identify the dereverberated transfer function $\widehat{G}_{\rm d}(z)$. Given a window size of 2Δ rad s^{-1}, the complex windowed average frequency response is given by

$$\overline{G}_{\rm d}(\mathrm{e}^{\jmath\theta}) = \frac{1}{\theta_{\min} - \theta_{\max}} \int_{\theta_{\max}}^{\theta_{\min}} G_{\rm d}(\mathrm{e}^{\jmath v})\,\mathrm{d}v, \tag{30}$$

where $\theta_{\min} \triangleq \min(\pi, \theta+\Delta)$ and $\theta_{\max} \triangleq \max(0, \theta-\Delta)$. The dereverberated transfer function $\widehat{G}_{\mathrm{d}}(z)$ is then constructed by fitting $\widehat{G}_{\mathrm{d}}(\mathrm{e}^{\jmath\theta})$ to $\overline{G}_{\mathrm{d}}(\mathrm{e}^{\jmath\theta})$ and enforcing asymptotic stability of $\widehat{G}_{\mathrm{d}}(z)$. The order is chosen to be as low as possible while still capturing the rolloff and phase characteristics of $\overline{G}_{\mathrm{d}}(\mathrm{e}^{\jmath\theta})$, and Δ is chosen such that all the modes in $G_{\mathrm{d}}(\mathrm{e}^{\jmath\theta})$ are smoothed out while maintaining the backbone of the response. The algorithm used to construct $\widehat{G}_{\mathrm{d}}(z)$ from $\overline{G}_{\mathrm{d}}(\mathrm{e}^{\jmath\theta})$ is given by Algorithm 1 of [20] except that the order of $\widehat{G}_{\mathrm{d}}(z)$ is fixed beforehand.

B. 20th-Order MISO System Example

Consider the system shown in Figure 3 with two inputs and one output. The system is lightly damped with the damping ratio varying between 1-17% with more than half of the modes having less than 2% damping. The dereverberated transfer function is created channel by channel for the inputs using each of the above methods. The system is discretized with a sample rate of $T_{\mathrm{s}} = 0.0005$ s.

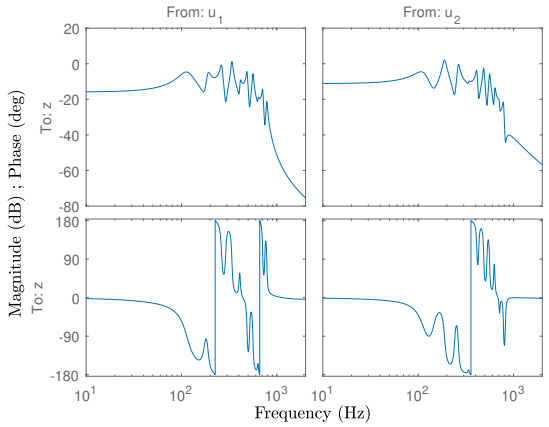

Fig. 3: 20th-order MISO system. The continuous-time system $G(s)$ has 2 inputs and one output. The dereverberated transfer function will be created by treating each channel as a SISO system.

Using $\Delta = 180\pi$ rad s^{-1} and $\hat{n}_{\max} = 4$ yields the system shown in Figure 4. From Figure 4, the complex windowed average frequency response does not capture the modes of the system. The window size of 180π rad s^{-1} creates multiple damped modes that are visible in the frequency response. Consequently, the spectral radius of the dereverberated transfer function resulting from averaging is reduced compared to $G_{\mathrm{d}}(z)$ and has complex poles with damping of 27.5% and 68.2%.

V. Example: Adaptive Disturbance Rejection Based on a Dereverberated Target Model

Let

$$G(s) = \frac{400\pi^2\omega_{\mathrm{p}}^2}{\omega_{\mathrm{z}}^2} \frac{s^2 + 2\zeta\omega_{\mathrm{z}}s + \omega_{\mathrm{z}}^2}{(s+10\pi)(s+40\pi)(s^2 + 2\zeta\omega_{\mathrm{p}}s + \omega_{\mathrm{p}}^2)} \tag{31}$$

and consider the block diagram in Figure 1 with $G(s) = G_{zu}(s) = G_{zw}(s) = G_{yu}(s) = G_{yw}(s)$, $T_{\mathrm{s}} = 0.01$ s, and $\omega_{\mathrm{p}} = 20\pi$ rad s^{-1}. The following subsections investigate the

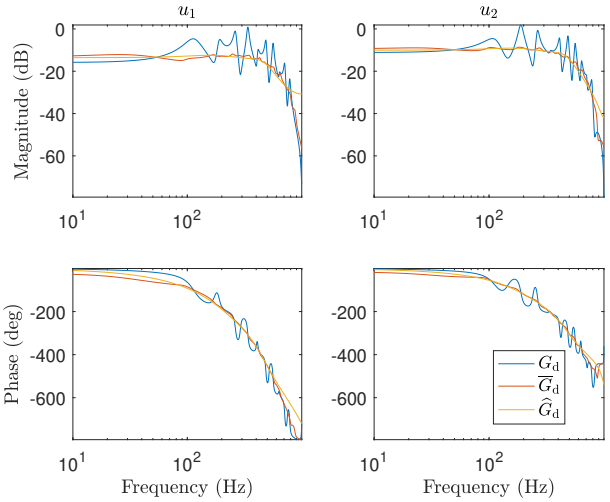

Fig. 4: Complex windowed average for the 20th-order MISO system. Frequency response of $\widehat{G}_{\mathrm{d}}(z)$, $\overline{G}_{\mathrm{d}}(z)$ and $\widehat{G}_{\mathrm{d}}(z)$. Notice that the phase of $\widehat{G}_{\mathrm{d}}(z)$ follows the general trend of the phase of $G_{\mathrm{d}}(z)$.

performance of RCAC when using a DTM for harmonic disturbance rejection on (31) for various disturbance frequencies and values of ω_{z} and ζ. The simulations are conducted in a sample-data feedback loop with integration between samples in order to capture the intersample behavior of the system. For each case, the harmonic disturbance frequency ω_{d} is swept from 4π to 50π rad s^{-1}, and the asymptotic error at the sample times is plotted against the magnitude and phase error between $G_{\mathrm{f}}(e^{\jmath\omega_{\mathrm{d}}T_{\mathrm{s}}})$ and $G_{zu,\mathrm{d}}(e^{\jmath\omega_{\mathrm{d}}T_{\mathrm{s}}})$.

The DTM is created using $\hat{n}_{\max} = 2$, $\Delta = 8\pi$ rad s^{-1}, and $\beta = 1$, with RCAC being initialized with $n_{\mathrm{c}} = 20$, $\theta_0 = 0_{l_\theta}$, $k_w = 5n_{\mathrm{c}}$, $\alpha = 0.5$, and $R = 0$. The resulting magnitude of the asymptotic closed-loop response at the sample times is plotted along with the magnitude error versus the phase error between $G_{\mathrm{f}}(e^{\jmath\omega_{\mathrm{d}}T_{\mathrm{s}}})$ and $G_{zu,\mathrm{d}}(e^{\jmath\omega_{\mathrm{d}}T_{\mathrm{s}}})$ for various values of ω_{z} and ζ in Figure 5. For the specific case where $\omega_{\mathrm{d}} = 21\pi$ rad s^{-1}, $\omega_{\mathrm{z}} = 22\pi$ rad s^{-1}, and $\zeta = 0.01$, the resulting DTM is shown in Figure 6 with the resulting closed-loop response in Figure 7.

VI. Experimental Application

RCAC using a dereverberated target model is now implemented in an acoustic experiment consisting of an omnidirectional microphone with three mid-bass speakers in a 6 ft $\times$ 3 ft $\times$ 3 ft enclosed space as shown in Figure 8. One speaker w is used to generate the harmonic disturbance, with the other two speakers u_1 and u_2 being available for control. RCAC is implemented using a dSPACE SCALEXIO at a sample rate of 8 kHz. The SCALEXIO is also used to generate the harmonic disturbance consisting of seven tones at 0.8, 0.9, 1.06, 1.3, 1.6, 2.2, and 3 kHz.

Due to the nature of the acoustic experiment, there were multi-sample delays in the system that needed to be characterized to facilitate creating the DTF. At 8 kHz, the delays from inputs u_1 and u_2 to the microphone corresponded to 9 and 16 samples respectively. After identifying a model of the experiment, a new model without the delays was created and used to generate the DTF. G_{f} was then created by scaling by β and adding the 9 and 16 sample delays to the appropriate inputs in the DTF.

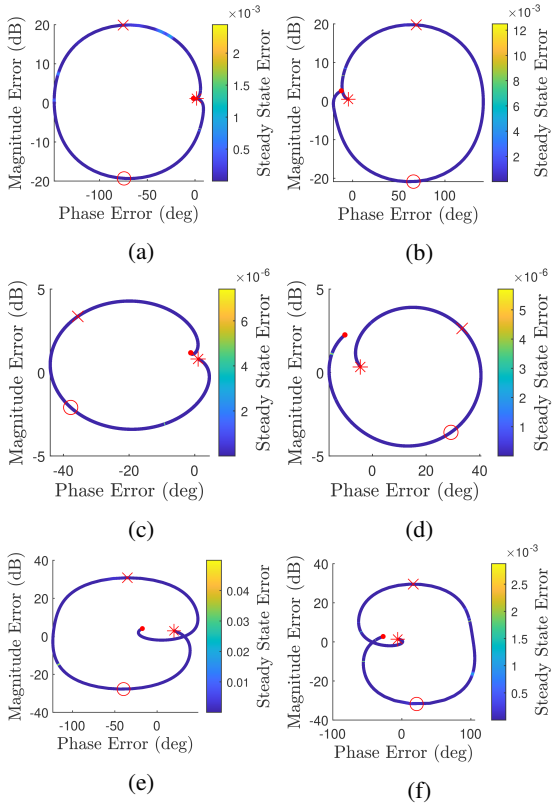

Fig. 5: Example: The above plots show the magnitude of the asymptotic closed-loop response at the sample times along with the magnitude error versus the phase error between $G_{\mathrm{f}}(e^{j\omega_{\mathrm{d}}T_{\mathrm{s}}})$ and $G_{zu,\mathrm{d}}(e^{j\omega_{\mathrm{d}}T_{\mathrm{s}}})$ as ω_{d} is swept from 4π to 50π rad s^{-1} for various values of ζ and ω_{z}. Here, "$\cdot$" corresponds to the 4π rad s^{-1} disturbance, "*" for the 50π rad s^{-1} disturbance, "x" for the damped frequency of the pole, and "o" for the damped frequency of the zero. a) $\zeta = 0.01$, $\omega_{\mathrm{z}} = 22\pi$ rad s^{-1}; b) $\zeta = 0.01$, $\omega_{\mathrm{z}} = 18\pi$ rad s^{-1}; c) $\zeta = 0.1$, $\omega_{\mathrm{z}} = 22\pi$ rad s^{-1}; d) $\zeta = 0.1$, $\omega_{\mathrm{z}} = 18\pi$ rad s^{-1}; e) $\zeta = 0.01$, $\omega_{\mathrm{z}} = 28\pi$ rad s^{-1}; f) $\zeta = 0.01$, $\omega_{\mathrm{z}} = 12\pi$ rad s^{-1}

Using $\hat{n}_{\max} = 6$, $\Delta = 1000\pi$ rad s^{-1}, and $\beta = 1$ yields the dereverberated target model shown in Figure 9. RCAC is initialized with $n_{\mathrm{c}} = 50$, $\theta_0 = 0_{l_\theta}$, $k_w = 11n_{\mathrm{c}}$, $\alpha = 0.05$, and $R = 0$. Figure 10 shows that RCAC is able to reject the disturbance as its coefficients converge.

VII. Conclusions and Future Research

In this paper, a method identifying dereverberated transfer functions was formulated. The frequency response of the resulting dereverberated transfer functions was compared to that of the plant, showing that the dereverberated transfer function approximately follows the phase and magnitude trend of the original lightly damped plant.

For harmonic disturbance rejection, retrospective cost adaptive control (RCAC) was applied to a fourth-order numerical example using a dereverberated transfer function as the closed-loop target model. Using the limited modeling information provided by the dereverberated target model, RCAC was able to suppress the harmonic disturbances in a sampled-data feedback loop for a range of disturbance frequencies, damping ratios, and zero locations. RCAC was then

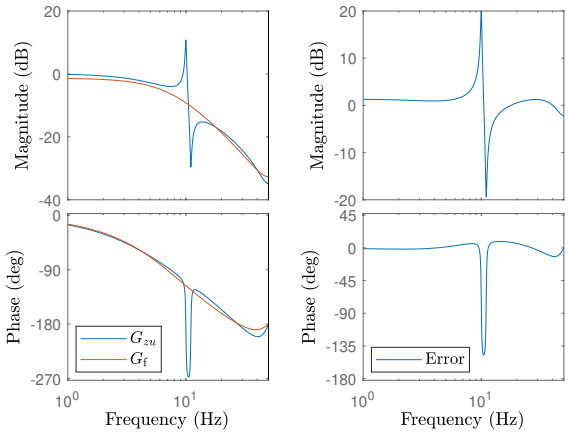

Fig. 6: Example: Complex windowed average with $\omega_{\mathrm{z}} = 22\pi$ rad s^{-1}, and $\zeta = 0.01$. a) the frequency response of the discretized G_{zu} and the DTM G_{f}. The DTM was constructed by using the complex windowed average method with $\hat{n}_{\max} = 2$, and $\Delta = 8\pi$ rad s^{-1}. b) the error between the frequency response of the discretized G_{zu} and G_{f}.

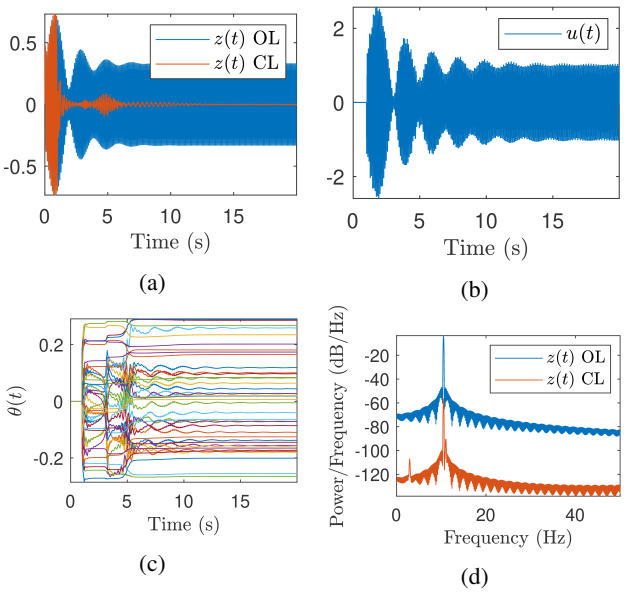

Fig. 7: Example: Closed-loop response with $\omega_{\mathrm{d}} = 21\pi$ rad s^{-1}, $\omega_{\mathrm{z}} = 22\pi$ rad s^{-1}, and $\zeta = 0.01$. a) shows the open-loop and closed-loop response of the system subject to the harmonic disturbance. RCAC starts at 1 s. b) shows RCAC's control input. c) shows the coefficients of RCAC as they converge. d) shows the power spectral density of both the open and closed-loop responses. Notice that the peak in the open-loop response corresponding to the disturbance is suppressed in the closed-loop response.

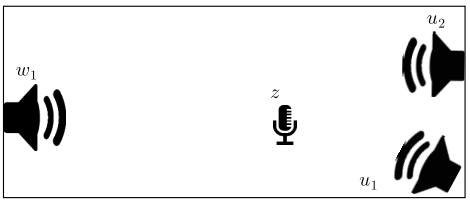

Fig. 8: Top-down view of the experimental setup.

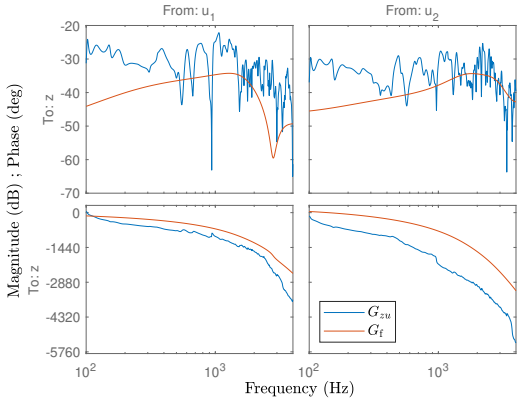

Fig. 9: Experiment: Complex windowed average. The frequency response of the discretized G_{zu} and the dereverberated target model G_{f} generated by using the complex windowed average method with $\hat{n}_{\max} = 6$, $\Delta = 1000\pi$ rad s^{-1}, and scaling the result by $\beta = 0.5$.

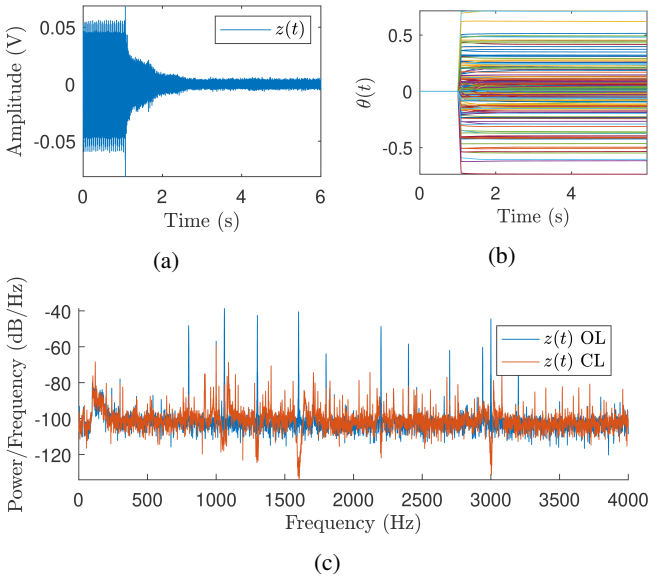

Fig. 10: Experiment: Closed-loop response. a) shows the initial open-loop response and the closed-loop response of the system subject to the harmonic disturbance once RCAC starts at 1.05 s. b) shows the coefficients of RCAC as they converge. c) shows the power spectral density of both the open and closed-loop responses. Notice that the 7 largest peaks in the open-loop response corresponding to the disturbance are suppressed in the closed-loop response to the noise floor. Tones from the laboratory environment are also present.

applied to a 2-input, single-output acoustic noise-suppression experiment using an identified dereverberated target model. The results show that a closed-loop dereverberated target that captures the phase and magnitude trend but not the detailed peaks and notches of the plant can be effective for lightly damped plants with harmonic disturbances.

Future work will consider broadband and nonstationary disturbances, as well as online identification of the dereverberated target model. A key challenge is to develop dereverberated target models to avoid the possibility of unstable pole-zero cancellation.

Acknowledgements

This work was supported by a NASA Space Technology Graduate Research Opportunity under grant number 80NSSC20K1164.

References

[1] C. R. Fuller and A. H. von Flotow, "Active control of sound and vibration," *IEEE Contr. Sys. Mag.*, vol. 15, no. 6, pp. 9–19, 1995.

[2] P. A. Nelson and S. J. Elliot, *Active Control of Sound*. Academic Press, 1992.

[3] S. M. Kuo and D. R. Morgan, *Active Noise Control Systems: Algorithms and DSP Implementations*. Wiley, 1995.

[4] A. Preumont, *Vibration Control of Active Structures: An Introduction*, 4th ed. Springer, 2018.

[5] D. Abramovitch and G. Franklin, "A brief history of disk drive control," *IEEE Contr. Sys. Mag.*, vol. 22, no. 3, pp. 28–42, 2002.

[6] M. M. Seron, J. H. Braslavsky, and G. C. Goodwin, *Fundamental Limitations in Filtering and Control*. New York: Springer, 1997.

[7] B. Widrow and S. D. Stearns, *Adaptive signal processing*. Prentice-Hall, 1985, vol. 15.

[8] S. M. Kuo and D. R. Morgan, "Active noise control: a tutorial review," *Proceedings of the IEEE*, vol. 87, no. 6, pp. 943–973, Jun 1999.

[9] R. L. Clark, W. R. Saunders, and G. P. Gibbs, *Adaptive Structures: Dynamics and Control*. Wiley, 2001.

[10] Y. Rahman, A. Xie, and D. S. Bernstein, "Retrospective Cost Adaptive Control: Pole Placement, Frequency Response, and Connections with LQG Control," *IEEE Contr. Sys. Mag.*, vol. 37, no. October, pp. 85–121, 2017.

[11] S. Dai, Z. Ren, and D. S. Bernstein, "Adaptive control of nonminimum-phase systems using shifted laurent series," *Int. J. Contr.*, vol. 90, pp. 409–422, 2017.

[12] D. G. MacMartin, "An H-infinity Power Flow Approach to Control of Uncertain Structures," Master's thesis, MIT, 1990.

[13] D. G. MacMartin and S. R. Hall, "Broadband control of flexible structures using statistical energy analysis concepts," *J. Guid. Cont. Dyn.*, vol. 17, pp. 361–369, 1994.

[14] E. Skudrzyk, "The mean-value method of predicting the dynamic response of complex vibrators," *J. Acoust. Soc. Am.*, vol. 67, pp. 1105–1135, 1980.

[15] K. Matsuda and H. A. Fujii, "Analysis of the dereverberated transfer function in finite dimensions," *J. Guid. Contr. Dyn.*, vol. 19, pp. 91–98, 1996.

[16] D. G. MacMartin, "A stochastic approach to broadband control of parametrically uncertain structures," Ph.D. dissertation, MIT, 1996.

[17] C. H. Hodges and J. Woodhouse, "Theories of noise and vibration transmission in complex structures," *Rep. Prog. Phys.*, vol. 49, pp. 107–170, 1986.

[18] M. Sidman, F. Verghese, and D. G.C., "Parametric system identification on logarithmic frequency response data," *IEEE Trans. Autom. Contr.*, vol. 36, pp. 1065–1070, 1991.

[19] J. B. Hoagg and D. S. Bernstein, "Nonminimum-Phase Zeros: Much to Do about Nothing," *IEEE Contr. Sys. Mag.*, vol. 27, no. June, pp. 45–57, 2007.

[20] T. McKelvey, H. Akcay, and L. Ljung, "Subspace-based multivariable system identification from frequency response data," *IEEE Trans. Autom. Contr.*, vol. 41, no. 7, pp. 960–979, Jul 1996.